

# Densely Supervised Grasp Detector (DSGD)

Umar Asif, Jianbin Tang, and Stefan Herrer

**Abstract**—This paper presents *Densely Supervised Grasp Detector (DSGD)*, a deep learning framework which combines CNN structures with layer-wise feature fusion and produces grasps and their confidence scores at different levels of the image hierarchy (i.e., global-, region-, and pixel-levels). Specifically, at the global-level, DSGD uses the entire image information to predict a grasp and its confidence score. At the region-level, DSGD uses a region proposal network to identify salient regions in the image and predicts a grasp for each salient region. At the pixel-level, DSGD uses a fully convolutional network and predicts a grasp and its confidence at every pixel. The grasp with the highest confidence score is selected as the output of DSGD. This selection from hierarchically generated grasp candidates overcomes limitations of the individual models. DSGD outperforms state-of-the-art methods on the Cornell grasp dataset in terms of grasp accuracy. Evaluation on a multi-object dataset and real-world robotic grasping experiments show that DSGD produces highly stable grasps on a set of unseen objects in new environments. It achieves 96% grasp detection accuracy and 90% robotic grasping success rate with real-time inference speed.

## I. INTRODUCTION

Grasp detection is a crucial task in robotic grasping because errors in this stage affect grasp planning and execution. A major challenge in grasp detection is generalization to unseen objects in the real-world. Recent advancements in deep learning have produced Convolutional Neural Network (CNN) based grasp detection methods which achieve higher grasp detection accuracy compared to hand-crafted features. Methods such as [1], [2] focused on learning grasps in a global-context (i.e., the model predicts one grasp considering the whole input image), through regression-based approaches (which directly regress the grasp parameters defined by the location, width, height, and orientation of a 2D rectangle in image space). Other methods such as [3] focused on learning grasps at patch-level by extracting patches (of different sizes) from the image and predicting a grasp for each patch. Recently, methods such as [4], [5] used auto-encoders to learn grasp parameters at each pixel in the image. They showed that one-to-one mapping (of image data to ground truth grasps) at the pixel-level can effectively be learnt using small CNN structures to achieve fast inference speed. These studies show that grasp detection performance is strongly influenced by three main factors: **i)** The choice of the CNN structure used for feature learning, **ii)** the objective function used to learn grasp representations, and **iii)** the image hierarchical context at which grasps are learnt (e.g., global or local). In the view of these, in this work, we

explore the advantages of combining multiple global and local grasp detectors and a mechanism to select the best grasp out of the ensemble. We also explore the benefits of learning grasp parameters using a combination of regression and classification objective functions. Finally, we explore different CNN structures as base networks to identify the best performing architecture in terms of inference speed and accuracy. The main contributions of this paper are summarized below:

- 1) We present *Densely Supervised Grasp Detector (DSGD)*, an ensemble of multiple CNN structures which generates grasps and their confidence scores at different levels of image hierarchy (i.e., global-, region-, and pixel-levels). The grasp with the highest confidence score is selected as the output.
- 2) We propose dense feature fusion within layers of our networks. This enables the networks to learn better image-to-grasp mappings compared to the models without feature fusion.
- 3) We propose a region-based grasp network, which learns to extract salient parts (e.g., handles or boundaries) from the input image, and use the information about these parts to learn class-agnostic grasps (i.e., each grasp is associated with a probability with respect to a graspable class and a non-graspable class).
- 4) We perform an ablation study of our DSGD by varying its critical parameters and present a grasp detector that achieves real-time speed and high grasp accuracy.
- 5) We demonstrate the robustness of DSGD for producing stable grasps for unseen objects in real-world environments using a multi-object dataset and robotic grasping experiments. See our experiment videos at: <https://tinyurl.com/y8csconx> and <https://tinyurl.com/y8muq32g>

## II. RELATED WORK

In the context of deep learning based grasp detection, methods such as [1], [6], [7] trained sliding window based grasp detectors. However, their high inference times limit their application for real-time systems. Other methods such as [8]–[10] reduced inference time by processing a discrete set of grasp candidates, but these methods ignore some potential grasps. Alternatively, methods such as [2], [11], [12] proposed end-to-end CNN-based approaches which regress a single grasp for an input image. However, these methods tend to produce average grasps which are invalid for certain symmetric objects [2]. Recently, methods such as [4], [5], [13]–[15] used auto-encoders to generate grasp poses at every pixel. They demonstrated higher grasp accuracy

compared to the global methods. Another stream of work focused on learning mapping between images of objects and robot motion parameters using reinforcement learning, where the robot iteratively refines grasp poses through real-world experiments. In this context, the method of [3] learned visual-motor control by performing more than 40k grasping trials on a real robot. The method of [16] learned image-to-gripper pose mapping using over 800k motor commands generated by 14 robotic arms performing grasping trials for over 2 months. In this paper, we present a grasp detector which has several key differences from the current grasp detection methods. **First**, our detector generates multiple global and local grasp candidates and selects the grasp with the highest quality. This allows our detector to effectively recover from the errors of the individual global or local models. **Second**, we introduce a region-based grasp network which learns grasps using information about salient parts of objects (e.g., handles, extrusions, or boundaries), and produces more accurate grasps compared to global [11] or local detectors [3]. **Finally**, we propose layer-wise feature fusion in the higher-level layers of CNN structures. This maximizes variation in the information flow across the networks and produces better image-to-grasp mappings compared to the models of [2], [4].

### III. PROBLEM FORMULATION

Given an image of an object as input, the goal is to generate grasps at different image hierarchical levels (i.e., global-, region- and pixel-levels), and select the grasp with the highest confidence as the output. We define the global grasp by a 2D oriented rectangle on the target object in the image space. It is given by:

$$\mathcal{G}_g = [x_g, y_g, w_g, h_g, \theta_g, \rho_g], \quad (1)$$

where  $x_g$  and  $y_g$  represent the centroid of the rectangle. The terms  $w_g$  and  $h_g$  represent the width and the height of the rectangle. The term  $\theta_g$  represents the angle of the rectangle with respect to x-axis. The term  $\rho_g$  is *grasp confidence* and represents the quality of a grasp. Our region-level grasp is defined by a class-agnostic representation, where the parameters of the rectangle are associated with  $n$  classes (a graspable class:  $n = 1$ , and a non-graspable class:  $n = 0$ ). It is given by:

$$\mathcal{G}_r = [x_r^n, y_r^n, w_r^n, h_r^n, \theta_r^n, \rho_r^n], n \in [0, 1]. \quad (2)$$

Our pixel-level grasp is defined as:

$$\mathcal{G}_p = [M_{xy}, M_w, M_h, M_\theta] \in \mathbb{R}^{s \times W \times H}, \quad (3)$$

where  $M_{xy}$ ,  $M_w$ ,  $M_h$ , and  $M_\theta$  represent  $\mathbb{R}^{s \times W \times H}$ -dimensional feature maps<sup>1</sup>, which encode the position, width, height, and orientation of grasps at every pixel of the image, respectively. The terms  $W$  and  $H$  represent the width and height of the input image respectively. We learn the grasp representations ( $\mathcal{G}_g$ ,  $\mathcal{G}_r$ , and  $\mathcal{G}_p$ ) using joint regression-classification based objective functions, where we regress the position, width, and the

height parameters using an Euclidean Loss, and classifies the grasp orientation with respect to  $N_\theta = 50$  classes (angular-bins) using a Cross Entropy Loss.

### IV. THE PROPOSED DSGD (FIG. 1)

Our DSGD is composed of four main modules as shown in Fig. 1: a base network for feature extraction, a Global Grasp Network (GGN) for producing a grasp at the image-level, a Region Grasp Network (RGN) for producing grasps using salient parts of the image, and a Pixel Grasp Network (PGN) for generating grasps at each image pixel. In the following, we describe in detail the various modules of DSGD.

#### A. Base Network

The purpose of the base network is to act as a feature extractor. We extract features from the intermediate layers of a CNN such as ResNets [18], and use the features to learn grasp representations at different hierarchical levels.

#### B. Dense Feature Fusion

To maximize variation in the information flow across the network, we introduce *Dense blocks* (4-7): bottleneck convolutions interconnected through dense connections, at the higher-levels of our networks as shown in Fig. 1. Specifically, a dense block consists of  $N_l$  number of layers termed *Dense Layers* which share information from all the preceding layers connected to the current layer through skip connections [17]. Fig. 3 shows the structure of a dense block with  $N_l = 6$  dense layers. Each dense layer consists of  $1 \times 1$  and  $3 \times 3$  convolutions followed by Batch Normalization [19] and a Rectified Linear Unit (ReLU). The output of the  $l^{th}$  dense layer ( $\mathcal{X}_l$ ) in a dense block can be written as:

$$\mathcal{X}_l = [\mathcal{X}_0, \dots, \mathcal{X}_{l-1}], \quad (4)$$

where  $[\dots]$  represents concatenation of the features produced by the layers  $0, \dots, l-1$ .

#### C. Global Grasp Network (GGN)

Our GGN structure is composed of two sub-networks as shown in Fig. 1-A: a Global Grasp Prediction Network (GGPN) for generating grasp pose ( $[x_g, y_g, w_g, h_g, \theta_g]$ ) and a Grasp Evaluation Network (GEN) for predicting grasp confidence ( $\rho_g$ ). The GGPN structure is composed of a dense block, an averaging operation, a 4-dimensional fully connected layer for predicting the parameters  $[x_g, y_g, w_g, h_g]$ , and a 50-dimensional fully connected layer for predicting  $\theta_g$ . The GEN structure is similar to GGPN except that GEN has a single 2-dimensional fully connected layer for predicting  $\rho_g$ . The input to GEN is a grasp image which is produced by replacing the *Blue* channel of the input image with a binary rectangle image generated from the output of GGPN as shown in Fig. 2. Let  $R_{g_i} = [x_{g_i}, y_{g_i}, w_{g_i}, h_{g_i}]$ ,  $\theta_{g_i}$  and  $\rho_{g_i}$  denote the predicted values of a global grasp for the  $i^{th}$  image. We define the loss of the GGPN and the GEN models over  $K$  images as:

$$L_{ggpn} = \sum_{i \in K} ((1 - \lambda_1) L_{reg}(R_{g_i}, R_{g_i}^*) + \lambda_1 L_{cls}(\theta_{g_i}, \theta_{g_i}^*)), \quad (5)$$

<sup>1</sup> $s = 1$  for  $M_{xy}$ ,  $M_w$ , and  $M_h$ , and  $s = 50$  for  $M_\theta$ .

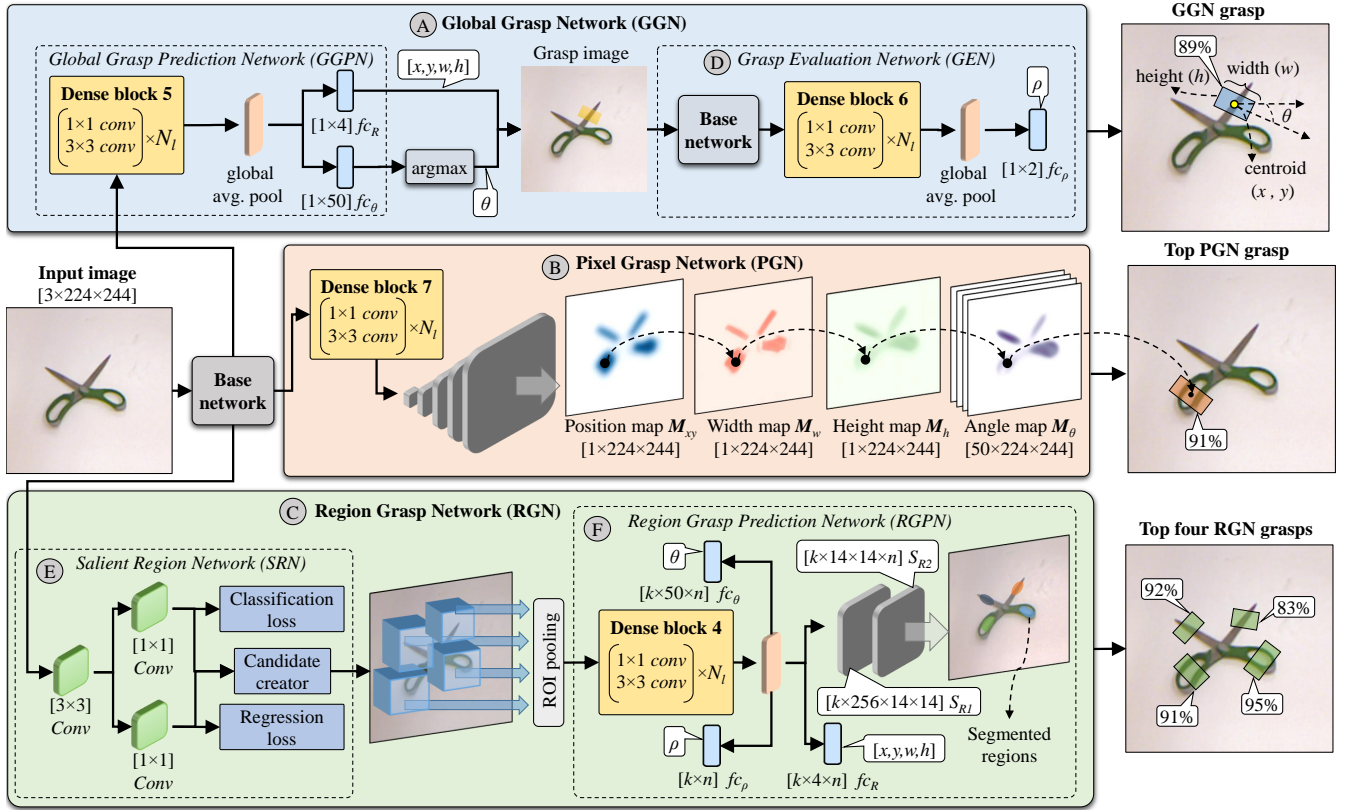


Fig. 1: Overview of our DSGD architecture. Given an image as input, DSGD uses a base network to extract features which are fed into a Global Grasp Network (A), a Pixel Grasp Network (B), and a Region Grasp network (C), to produce grasp candidates. The global model produces a single grasp per image and uses an independent Grasp Evaluation Network (D) to produce grasp confidence. The pixel-level model uses a fully convolutional network and produces grasps at every pixel. The region-level model uses a Salient Region Network (E) to extract salient parts of the image and uses information about these parts to produce grasps. The grasp with the highest score is selected as the output.

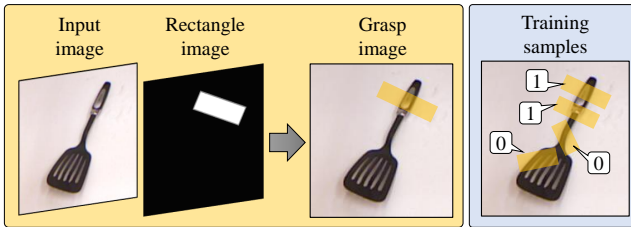


Fig. 2: Left: A grasp image is generated by replacing the blue channel of the input image with a binary rectangle image produced from a grasp pose. Right: Our Grasp Evaluation Network is trained using grasp images labelled in terms of valid (1) and invalid (0) grasp rectangles.

$$L_{gen} = \sum_{i \in K} L_{cls}(\rho_{g_i}, \rho_{g_i}^*), \quad (6)$$

where  $R_{g_i}^*$ ,  $\theta_{g_i}^*$ , and  $\rho_{g_i}^*$  represent the ground-truths. The term  $L_{reg}$  is a regression loss defined as:

$$L_{reg}(R, R^*) = \|R - R^*\| / \|R^*\|_2. \quad (7)$$

The term  $L_{cls}$  is a classification loss defined as:

$$L_{cls}(x, c) = - \sum_{c=1}^{N_\theta} \mathcal{Y}_{x,c} \log(p_{x,c}), \quad (8)$$

where  $\mathcal{Y}$  is a binary indicator if class label  $c$  is the correct classification for observation  $x$ , and  $p$  is the predicted probability of observation  $x$  of class  $c$ .

#### D. Region Grasp Network (RGN)

The RGN structure is composed of two sub-networks as shown in Fig. 1-C: a Salient Region Network (SRN) for extracting salient parts of image, and a region grasp prediction network (RGP) for predicting a grasp for each candidate salient part.

1) *Salient Region Network (SRN)*:: Here, we use the features extracted from the base network to generate regions defined by the location  $(x_{sr}, y_{sr})$ , width  $(w_{sr})$ , height  $(h_{sr})$ , and confidence  $(\rho_{sr})$  of non-oriented rectangles which encompass salient parts of the image (e.g., handles, extrusions, or boundaries). For this, we first generate a fixed number of rectangles using the Region of Interest (ROI) method of [20]. Next, we use the features from the base network and optimize a Mean Squared Loss on the rectangle coordinates and a Cross Entropy Loss on the rectangle confidence scores. Let  $T_i = [x_{sr}, y_{sr}, w_{sr}, h_{sr}]$  denote the parameters of the  $i^{th}$  predicted rectangle, and  $\rho_{sr_i}$  denote its probability whether it belongs to a graspable region or a non-graspable region.

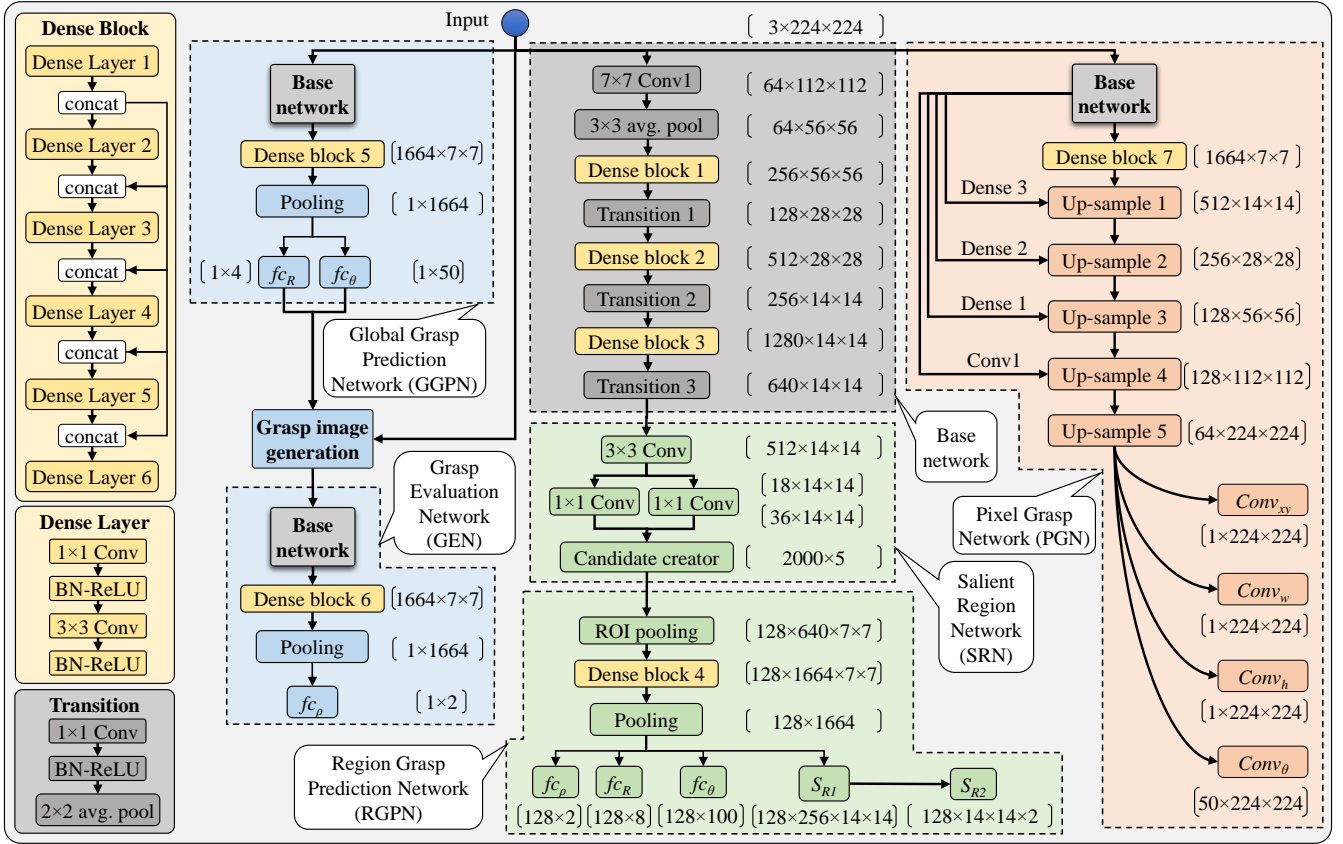


Fig. 3: Detailed architecture of our DSGD with a DenseNet [17] as its base network.

The loss of SRN over  $\mathbf{I}$  proposals is given by:

$$L_{srn} = \sum_{i \in \mathbf{I}} ((1 - \lambda_2) L_{reg}(T_i, T_i^*) + \lambda_2 L_{cls}(\rho_{sr_i}, \rho_{sr_i}^*)), \quad (9)$$

where  $\rho_{sr_i}^* = 0$  for a non-graspable region and  $\rho_{sr_i}^* = 1$  for a graspable region. The term  $T_i^*$  represents the ground truth candidate corresponding to  $\rho_{sr_i}^*$ .

2) *Region Grasp Prediction Network (RGPN)*:: Here, we produce grasp poses for the salient regions predicted by SRN ( $k = 128$  in our implementation). For this, we crop features from the output feature maps of the base network using the Region of Interest (ROI) pooling method of [20]. The cropped features are then fed to *Dense block 4* which produces feature maps of  $k \times 1664 \times 7 \times 7$ -dimensions as shown in Fig. 3. These feature maps are then squeezed to  $k \times 1664$ -dimensions through a global average pooling, and fed to three fully connected layers  $fc_R \in \mathbb{R}^{k \times 4 \times n}$ ,  $fc_\theta \in \mathbb{R}^{k \times 50 \times n}$ , and  $fc_\rho \in \mathbb{R}^{k \times 2}$  which produce class-agnostic grasps. RGPN also has a segmentation branch (with two upsampling layers  $S_{R1} \in \mathbb{R}^{k \times 256 \times 14 \times 14}$  and  $S_{R2} \in \mathbb{R}^{k \times 14 \times 14 \times n}$ ), which produces a segmentation mask for each salient region as shown in Fig. 1-F. Let  $R_{r_i} = [x_{r_i}, y_{r_i}, w_{r_i}, h_{r_i}]$ ,  $\theta_{r_i}$ , and  $\rho_{r_i}$  denote the predicted values of a region-level grasp for the  $i^{th}$  salient region, and  $\mathcal{S}_i \in \mathbb{R}^{14 \times 14 \times n}$  denotes the corresponding predicted segmentation. The loss of the RGPN model is defined over  $\mathbf{I}$  salient regions

as:

$$L_{rgpn} = \sum_{i \in \mathbf{I}} (L_{reg}(R_{r_i}, R_{r_i}^*) + \lambda_3 L_{cls}(\theta_{r_i}, \theta_{r_i}^*) + \lambda_3 L_{cls}(\rho_{r_i}, \rho_{r_i}^*) + L_{seg}(\mathcal{S}_i, \mathcal{S}_i^*)), \quad (10)$$

where  $R^*$ ,  $\theta^*$ ,  $\rho^*$ , and  $\mathcal{S}^*$  represent the ground truths. The term  $\rho_{r_i}^* = 0$  for a non-graspable region and  $\rho_{r_i}^* = 1$  for a graspable region. The term  $L_{seg}$  represents a pixel-wise binary cross-entropy loss used to learn segmentations of salient regions. It is given by:

$$L_{seg} = -\frac{1}{|\mathcal{S}_i|} \sum_{j \in \mathcal{S}_i} (y_j \log(\hat{y}_j) + (1 - y_j) \log(1 - \hat{y}_j)), \quad (11)$$

where,  $y_j$  represents the ground truth value and  $\hat{y}_j$  denotes the predicted value for a pixel  $j \in \mathcal{S}_i$ . Learning segmentations in parallel with grasp poses helps the network to produce better localization results [20]. The total loss of our RGN model is given by:

$$L_{rgn} = L_{srn} + L_{rgpn}. \quad (12)$$

The terms  $\lambda_1$ ,  $\lambda_2$ , and  $\lambda_3$  in Eq. 5, Eq. 11, and Eq. 10 control the relative influence of classification over regression on the combined objective functions<sup>2</sup>.

<sup>2</sup>For experiments, we set the parameters  $\lambda_1$ ,  $\lambda_2$ , and  $\lambda_3$  to 0.4.

### E. Pixel Grasp network (PGN)

Here, we feed the features extracted from the base network into *Dense block 7* followed by a group of upsampling layers which increase the spatial resolution of the features and produce feature maps of the size of the input image. These feature maps encode the parameters of the grasp pose at every pixel of the image. Let  $M_{xy_i}$ ,  $M_{w_i}$ ,  $M_{h_i}$ , and  $M_{\theta_i}$  denote the predicted feature maps of the  $i^{th}$  image, respectively. We define the loss of the PGN model over  $K$  images as:

$$L_{pgn} = \sum_{i \in K} (L_{reg}(M_{xy_i}, M_{xy_i}^*) + L_{reg}(M_{w_i}, M_{w_i}^*) + L_{reg}(M_{h_i}, M_{h_i}^*) + L_{cls}(M_{\theta_i}, M_{\theta_i}^*)), \quad (13)$$

where  $M_{xy_i}^*$ ,  $M_{w_i}^*$ ,  $M_{h_i}^*$ , and  $M_{\theta_i}^*$  represent the ground-truths.

### F. Training and Implementation

For the global model, we trained the GGPN and the GEN sub-networks independently. For the region-based and the pixel-based models, we trained the networks in an end-to-end manner. Specifically, we initialized the weights of the base network with the weights pre-trained on ImageNet. For the *Dense blocks (4-7)*, the fully connected layers of GGPN, GEN, SRN, and RGN, and the fully convolutional layers of PGN, we initialized the weights from zero-mean Gaussian distributions (standard deviation set to 0.01, biases set to 0), and trained the networks using the loss functions in Eq. 5, Eq. 6, Eq. 11, Eq. 12, and Eq. 13, respectively for 150 epochs. The starting learning rate was set to 0.01 and divided by 10 at 50% and 75% of the total number of epochs. The parameter decay was set to 0.0005 on the weights and biases. Our implementation is based on the framework of Torch library [21]. Training was performed using ADAM optimizer with a batch size of 64.

## V. EXPERIMENTS

We evaluated DSGD for grasp detection on the popular Cornell grasp dataset [1], which contains 885 RGB-D images of 240 objects. The ground-truth is available in the form of grasp-rectangles. We also evaluated DSGD for multi-object grasp detection in new environments. For this, we generated a multi-object dataset which consists of 7000 RGB-D images of indoor scenes containing multiple objects placed in different locations and orientations. For evaluation, we used the object-wise splitting criteria [1] for both the Cornell grasp dataset and our multi-object dataset. The object-wise splitting splits the object instances randomly into train and test subsets (i.e., the training set and the test set do not share any images from the same object). This strategy evaluates how well the model generalizes to unseen objects. For comparison purposes, we followed the procedure of [2] and substituted the blue channel with the depth image, where the depth values are normalized between 0 and 255. We also performed data augmentation through random rotations. For grasp evaluation, we used the “rectangle-metric” proposed in

TABLE I: Grasp evaluation on the Cornell grasp dataset in terms of average grasp detection accuracy (%) and inference speed (*fps*).

Method	Accuracy	Speed
(Jiang <i>et. al.</i> 2011) Fast search	58.3	0.02
(Lenz <i>et. al.</i> 2015) Deep learning	75.6	0.07
(Redmon <i>et. al.</i> 2015) MultiGrasp	87.1	3.31
(Wang <i>et. al.</i> 2015) Multi-modal	-	7.10
(Kumra <i>et. al.</i> 2017) ResNets	88.9	16.03
(Guo <i>et. al.</i> 2017) Hybrid-Net	89.1	-
(this work) DSGD	<b>98.7</b>	8
(this work) DSGD-lite	92.2	<b>20</b>

TABLE II: Comparison of the individual networks of the proposed DSGD in terms of grasp accuracy (%) on the Cornell grasp dataset.

Base network	Global GGN	Local models		DSGD	
		PGN	RGN	No fusion	Fusion
SqueezeNet	83.7	84.8	85.6	85.9	<b>86.3</b>
VGG16	86.1	87.1	88.2	88.0	<b>89.3</b>
MobileNet	86.8	87.9	88.3	88.1	<b>89.4</b>
ResNet101	87.3	88.4	93.4	95.2	<b>96.8</b>
DenseNet169	88.7	90.5	95.6	97.3	<b>98.7</b>

[7]. A grasp is considered to be correct if: **i)** the difference between the predicted grasp angle and the ground-truth is less than  $30^\circ$ , and **ii)** the Jaccard index of the predicted grasp and the ground-truth is higher than 25%. The Jaccard index for a predicted rectangle  $\mathcal{R}$  and a ground-truth rectangle  $\mathcal{R}^*$  is defined as:

$$J(\mathcal{R}^*, \mathcal{R}) = |\mathcal{R}^* \cap \mathcal{R}| / |\mathcal{R}^* \cup \mathcal{R}|. \quad (14)$$

### A. Results

Table I shows that our DSGD achieved a considerable improvement of 9.3% in mean accuracy compared to the best performing model of [12] on the Cornell grasp dataset. We attribute this improvement to two main reasons: **First**, the proposed hierarchical grasp generation enables DSGD to produce grasps and their confidence scores from both global and local contexts. This enables DSGD to effectively recover from the errors of the global [11] or local methods [12]. **Second**, the use of dense feature fusion enables our networks to learn more discriminative features compared to the models used in [11], [12], respectively. From Table I, we also see that a *lite* version of our detector (DSGD-*lite*) can run at 20*fps* on a single GPU with competitive accuracy compared to the other methods, making it suitable for real-time applications. Fig. 4 shows grasps produced by our DSGD on some images of the Cornell grasp dataset.

1) *Significance of Combining Global and Local Models*:: Table II shows a quantitative comparison of the individual models of our DSGD in terms of grasp accuracy on the Cornell grasp dataset, for different CNN structures as the base network. The base networks we tested include: SqueezeNet [22], MobileNet [23], VGG16 [24], ResNets [18], and DenseNets [17]. Table II shows that on average the local models (PGN and RGN) produced higher grasp accuracy compared to the global model (GGN). The global



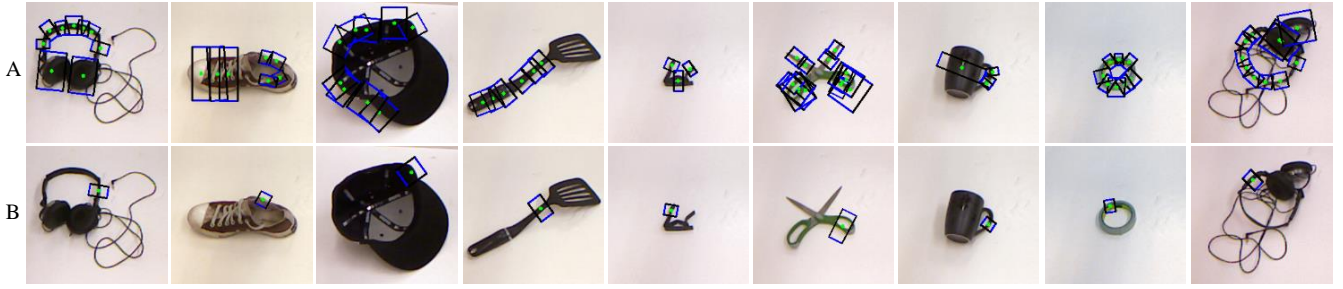


Fig. 4: Grasp detection results of our DSGD (B) on some challenging objects of the Cornell grasp dataset. Ground truths are shown in A.

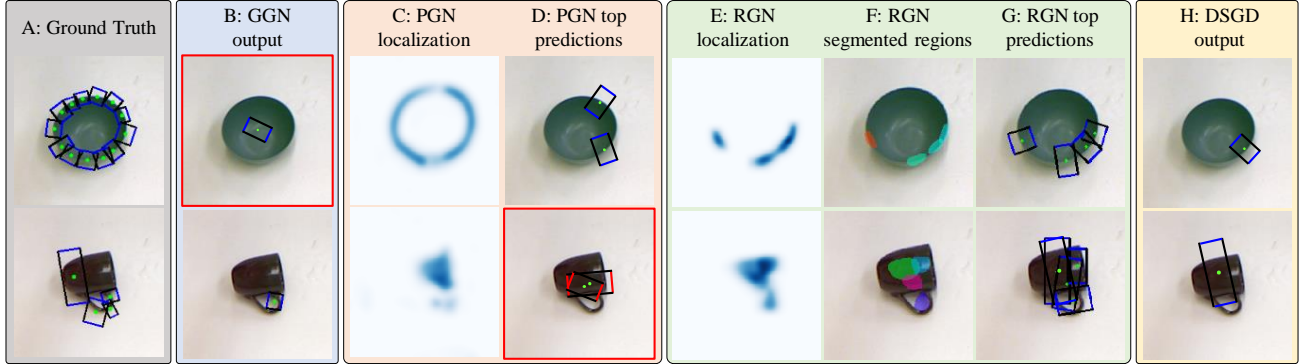


Fig. 5: Qualitative comparison of grasps produced by the proposed GGN, PGN, RGN, and DSGD models. The results show that our DSGD effectively recovers from the errors of the individual models. Incorrect predictions are highlighted in red.

and the local models have their own pros and cons. The global model learns an average of the ground-truth grasps from the global perspective. Although, the global-grasps are accurate for most of the objects, they tend to lie in the middle of circular symmetric objects resulting in localization errors as highlighted in red in Fig. 5-B. The PGN model on the other hand operates at the pixel-level and produces correct grasp localizations for these challenging objects as shown in Fig. 5-C. However, pixel-based model is susceptible to outliers in the position prediction maps which result in localization errors as highlighted in red in Fig. 5-D. Our RGN model works at a semi-global level while maintaining large receptive fields. It produces predictions using features extracted from the salient parts of the image which highly likely encode graspable parts of an object (e.g., handles or boundaries) as shown in Fig. 5-F. Consequently, RGN is less susceptible to pixel-level outliers and does not suffer global averaging errors as shown in Fig. 5-G. Our DSGD takes advantage of both the global context and local predictions and produces highly accurate grasps as shown in Fig. 5-H.

2) *Significance of Dense Feature Fusion*:: Here we investigate the significance of the proposed dense blocks (4-7) of our DSGD. Table II shows that using bottleneck convolutions with dense feature fusion at the higher-level layers produces improvements in grasp accuracy for all the tested base networks. For instance, DSGD with dense feature fusion produces 1.6% and 1.4% higher accuracy with ResNet and DenseNet base networks, respectively, compared to DSGD without dense feature fusion.

TABLE III: Ablation study of our DSGD on the Cornell grasp dataset in terms of the growth rate ( $\mathcal{W}$ ) and the number of dense layers.

Model	Growth rate ( $\mathcal{W}$ )	No. of Layers ( $N_l$ )	Accuracy (%)	No. of params.	Speed fps
DSGD-lite	12	6	92.2	<b>1.67</b>	<b>20</b>
DSGD-B	32	6	98.4	11.55	12
DSGD-C	32	12	98.5	21.47	10
DSGD-D	32	24	<b>98.7</b>	33.41	8
DSGD-E	48	32	98.7	40.97	6

### B. Ablative Study of the Proposed DSGD

a) *Growth Rate*:: The growth rate parameter  $\mathcal{W}$  refers to the number of output feature maps of each dense layer and therefore controls the depth of the network. Table III shows that a large growth rate is found to be significantly better, where the increase of  $\mathcal{W}$  from 12 to 32 increases average accuracy from 92.2% to 98.7%, at the expense of low runtime speed (e.g., 6 fps with  $\mathcal{W}=48$  vs. 20 fps with  $\mathcal{W}=12$ ) and more trainable parameters (e.g., 40.97 million vs. 1.67 million) due to the overhead from additional channels.

b) *Number of Dense Layers*:: Table III shows that wider dense blocks (i.e., more number of layers in the dense blocks) produce slight improvement in the overall accuracy (around 0.3% from DSGD-B to DSGD-E).

### C. Multi-Object Grasp Detection

Table IV shows our grasp evaluation on the multi-object dataset. The results show that on average, our DSGD improves grasp detection accuracy by 9% and 2.4% compared

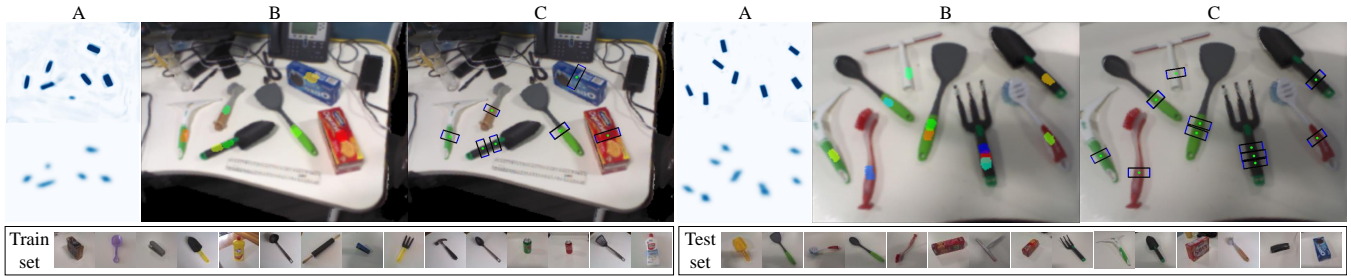


Fig. 6: Grasp evaluation on our multi-object dataset. The train and the test sets do not share any images from the same object instance. The localization outputs of our pixel-level (PGN) and region-level (RGN) grasp models are shown in (A). The segmented regions produced by our RGN model are shown in (B). Note that we only show grasps with confidence scores higher than 90% in (C). Our grasp detection results on Kinect video streams are available at: <https://tinyurl.com/y8muq32g>

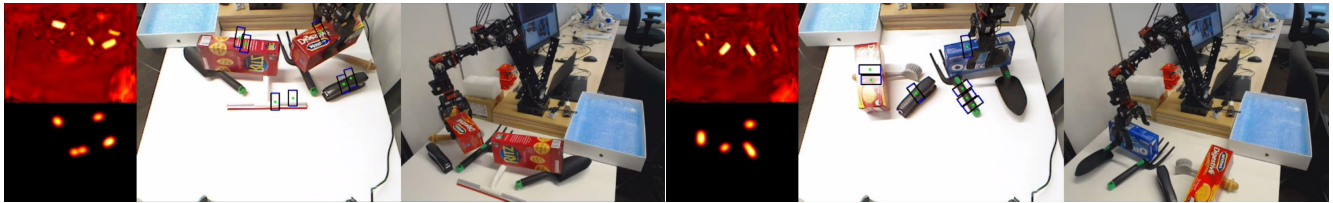


Fig. 7: Experimental setting for real-world robotic grasping. See video of our experiments at: <https://tinyurl.com/y8csconx>

TABLE IV: Grasp evaluation on our multi-object dataset.

Base network	Grasp accuracy			Robotic grasp success
	PGN	RGN	DSGD	
ResNet101	86.5%	93.4%	<b>95.8%</b>	89%
DenseNet169	87.4%	94.7%	<b>97.2%</b>	90%

to the pixel-level and region-level models, respectively. Fig. 6 shows qualitative results on the images of our multi-object dataset. The results show that our DSGD successfully generates correct grasps for multiple objects in real-world scenes containing background clutter. This justifies the practicality of our DSGD for real-world robotic grasping.

#### D. Robotic Grasping

Our robotic grasping setup consists of a Kinect for image acquisition and a 7 degrees of freedom robotic arm which is tasked to grasp, lift, and take-away the objects placed within the robot workspace. For each image, DSGD generates multiple grasp candidates as shown in Fig. 7. For grasp execution, we select a random candidate which is located within the robot workspace and has confidence greater than 90%. A robotic grasp is considered successful if the robot grasps a target object (verified through force sensing in the gripper), holds it in air for 3 seconds and takes it away from the robot workspace. The objects are placed in random positions and orientations to remove bias related to the object pose. Table IV shows the success rates computed over 200 grasping trials. The results show that we achieved grasp success rates of 90% with DenseNets as the base network. Some failure cases include objects with non-planar grasping surfaces (e.g., brush). However, this can be improved by multi-finger grasps. We leave this for future work as our

robotic arm only supports parallel grasps.

#### VI. CONCLUSION AND FUTURE WORK

We presented *Densely Supervised Grasp Detector* (DSGD), which generates grasps and their confidence scores at different image hierarchical levels (i.e., global-, region-, and pixel-levels). Our DSGD incorporates dense feature fusion on top of a base CNN network to maximize variation in information flow across the network. Experiments show that our proposed hierarchical grasp generation and dense feature fusion produces superior grasp accuracy compared to the state-of-the-art on the Cornell grasp dataset. Our evaluations on videos from Kinect and robotic grasping experiments show the capability of our DSGD for producing stable grasps for unseen objects in new environments. In future, we plan to reduce the computational burden of our DSGD through parameter-pruning for low-powered GPU devices.

#### REFERENCES

- [1] Lenz, I., Lee, H., Saxena, A.: Deep learning for detecting robotic grasps. *IJRR* 34(4-5) (2015) 705–724
- [2] Redmon, J., Angelova, A.: Real-time grasp detection using convolutional neural networks. In: *Proceedings of the IEEE International Conference on Robotics and Automation*, IEEE (2015) 1316–1322
- [3] Pinto, L., Gupta, A.: Supersizing self-supervision: Learning to grasp from 50k tries and 700 robot hours. In: *Proceedings of the IEEE International Conference on Robotics and Automation*, IEEE (2016) 3406–3413
- [4] Morrison, D., Corke, P., Leitner, J.: Closing the loop for robotic grasping: A real-time, generative grasp synthesis approach. *arXiv preprint arXiv:1804.05172* (2018)
- [5] Zeng, A., Song, S., Yu, K.T., Donlon, E., Hogan, F.R., Bauza, M., Ma, D., Taylor, O., Liu, M., Romo, E., et al.: Robotic pick-and-place of novel objects in clutter with multi-affordance grasping and cross-domain image matching. *arXiv preprint arXiv:1710.01330* (2017)

- [6] Saxena, A., Driemeyer, J., Ng, A.Y.: Robotic grasping of novel objects using vision. *IJRR* 27(2) (2008) 157–173
- [7] Jiang, Y., Moseson, S., Saxena, A.: Efficient grasping from rgbd images: Learning using a new rectangle representation. In: *Proceedings of the IEEE International Conference on Robotics and Automation*, IEEE (2011) 3304–3311
- [8] Mahler, J., Pokorny, F.T., Hou, B., Roderick, M., Laskey, M., Aubry, M., Kohlhoff, K., Kröger, T., Kuffner, J., Goldberg, K.: Dex-net 1.0: A cloud-based network of 3d objects for robust grasp planning using a multi-armed bandit model with correlated rewards. In: *Robotics and Automation (ICRA), 2016 IEEE International Conference on*, IEEE (2016) 1957–1964
- [9] Mahler, J., Liang, J., Niyaz, S., Laskey, M., Doan, R., Liu, X., Ojea, J.A., Goldberg, K.: Dex-net 2.0: Deep learning to plan robust grasps with synthetic point clouds and analytic grasp metrics. *Robotics: Science and Systems (RSS)* (2017)
- [10] Johns, E., Leutenegger, S., Davison, A.J.: Deep learning a grasp function for grasping under gripper pose uncertainty. In: *IROS, IEEE* (2016) 4461–4468
- [11] Kumra, S., Kanan, C.: Robotic grasp detection using deep convolutional neural networks. In: *IROS, IEEE* (2017)
- [12] Guo, D., Sun, F., Liu, H., Kong, T., Fang, B., Xi, N.: A hybrid deep architecture for robotic grasp detection. In: *Robotics and Automation (ICRA), 2017 IEEE International Conference on*, IEEE (2017) 1609–1614
- [13] Zeng, A., Song, S., Yu, K.T., Donlon, E., Hogan, F.R., Bauza, M., Ma, D., Taylor, O., Liu, M., Romo, E., Fazeli, N., Alet, F., Dafle, N.C., Holladay, R., Morona, I., Nair, P.Q., Green, D., Taylor, I., Liu, W., Funkhouser, T., Rodriguez, A.: Robotic pick-and-place of novel objects in clutter with multi-affordance grasping and cross-domain image matching. In: *Proceedings of the IEEE International Conference on Robotics and Automation*. (2018)
- [14] Myers, A., Teo, C.L., Fermüller, C., Aloimonos, Y.: Affordance detection of tool parts from geometric features. In: *Proceedings of the IEEE International Conference on Robotics and Automation*. (2015) 1374–1381
- [15] Varley, J., Weisz, J., Weiss, J., Allen, P.: Generating multi-fingered robotic grasps via deep learning. In: *Intelligent Robots and Systems (IROS), 2015 IEEE/RSJ International Conference on*, IEEE (2015) 4415–4420
- [16] Levine, S., Pastor, P., Krizhevsky, A., Ibarz, J., Quillen, D.: Learning hand-eye coordination for robotic grasping with deep learning and large-scale data collection. *IJRR* (2016) 0278364917710318
- [17] Huang, G., Liu, Z., Weinberger, K.Q., van der Maaten, L.: Densely connected convolutional networks. In: *Proceedings of the IEEE conference on computer vision and pattern recognition*. Volume 1. (2017) 3
- [18] He, K., Zhang, X., Ren, S., Sun, J.: Deep residual learning for image recognition. In: *CVPR*. (2016) 770–778
- [19] Ioffe, S., Szegedy, C.: Batch normalization: Accelerating deep network training by reducing internal covariate shift. In: *ICML*. (2015) 448–456
- [20] He, K., Gkioxari, G., Dollár, P., Girshick, R.: Mask r-cnn. In: *Computer Vision (ICCV), 2017 IEEE International Conference on*, IEEE (2017) 2980–2988
- [21] Paszke, A., Gross, S., Chintala, S., Chanan, G., Yang, E., DeVito, Z., Lin, Z., Desmaison, A., Antiga, L., Lerer, A.: Automatic differentiation in pytorch. (2017)
- [22] Iandola, F.N., Han, S., Moskewicz, M.W., Ashraf, K., Dally, W.J., Keutzer, K.: Squeezenet: Alexnet-level accuracy with 50x fewer parameters and 0.5mb model size. *arXiv preprint arXiv:1602.07360* (2016)
- [23] Howard, A.G., Zhu, M., Chen, B., Kalenichenko, D., Wang, W., Weyand, T., Andreetto, M., Adam, H.: Mobilenets: Efficient convolutional neural networks for mobile vision applications. *arXiv preprint arXiv:1704.04861* (2017)
- [24] Simonyan, K., Zisserman, A.: Very deep convolutional networks for large-scale image recognition. *arXiv preprint arXiv:1409.1556* (2014)